DESY 96-224
October 1996

ISSN 0418-nnnn

Scale Influence on the Energy Dependence of Photon-Proton Cross Sections

H1 Collaboration

Abstract

The scale dependence of the evolution of photoproduction cross sections with the photon-proton centre of mass energy W is studied using low $Q^2 < 0.01$ GeV^2 e^+p interactions collected by the H1 experiment at HERA. The value of the largest transverse momentum of a charged particle in the photon fragmentation region is used to define the hard scale. The slope of the W dependence of the cross section is observed to increase steeply with increasing transverse momentum. The result is compared to measurements of the Q^2 evolution of the W dependence of the virtual photon-proton cross section. Interpretations in terms of QCD and in terms of Regge phenomenology are discussed.

S. Aid[13], M. Anderson[23], V. Andreev[26], B. Andrieu[29], A. Babaev[25], J. Bähr[36], J. Bán[18], Y. Ban[28], P. Baranov[26], E. Barrelet[30], R. Barschke[11], W. Bartel[11], M. Barth[4], U. Bassler[30], H.P. Beck[38], M. Beck[14], H.-J. Behrend[11], A. Belousov[26], Ch. Berger[1], G. Bernardi[30], G. Bertrand-Coremans[4], M. Besançon[9], R. Beyer[11], P. Biddulph[23], P. Bispham[23], J.C. Bizot[28], V. Blobel[13], K. Borras[8], V. Boudry[29], A. Braemer[15], W. Braunschweig[1], V. Brisson[28], W. Brückner[14], P. Bruel[29], D. Bruncko[18], C. Brune[16], R. Buchholz[11], L. Büngener[13], J. Bürger[11], F.W. Büsser[13], A. Buniatian[4,39], S. Burke[19], M.J. Burton[23], D. Calvet[24], A.J. Campbell[11], T. Carli[27], M. Charlet[11], D. Clarke[5], A.B. Clegg[19], B. Clerbaux[4], S. Cocks[20], J.G. Contreras[8], C. Cormack[20], J.A. Coughlan[5], A. Courau[28], M.-C. Cousinou[24], G. Cozzika[9], L. Criegee[11], D.G. Cussans[5], J. Cvach[31], S. Dagoret[30], J.B. Dainton[20], W.D. Dau[17], K. Daum[42], M. David[9], C.L. Davis[19], B. Delcourt[28], A. De Roeck[11], E.A. De Wolf[4], M. Dirkmann[8], P. Dixon[19], P. Di Nezza[33], W. Dlugosz[7], C. Dollfus[38], K.T. Donovan[21], J.D. Dowell[3], H.B. Dreis[2], A. Droutskoi[25], O. Dünger[13], H. Duhm[12,†] J. Ebert[35], T.R. Ebert[20], G. Eckerlin[11], V. Efremenko[25], S. Egli[38], R. Eichler[37], F. Eisele[15], E. Eisenhandler[21], E. Elsen[11], M. Erdmann[15], W. Erdmann[37], A.B. Fahr[13], L. Favart[28], A. Fedotov[25], R. Felst[11], J. Feltesse[9], J. Ferencei[18], F. Ferrarotto[33], K. Flamm[11], M. Fleischer[8], M. Flieser[27], G. Flügge[2], A. Fomenko[26], J. Formánek[32], J.M. Foster[23], G. Franke[11], E. Fretwurst[12], E. Gabathuler[20], K. Gabathuler[34], F. Gaede[27], J. Garvey[3], J. Gayler[11], M. Gebauer[36], H. Genzel[1], R. Gerhards[11], A. Glazov[36], L. Goerlich[6], N. Gogitidze[26], M. Goldberg[30], D. Goldner[8], K. Golec-Biernat[6], B. Gonzalez-Pineiro[30], I. Gorelov[25], C. Grab[37], H. Grässler[2], T. Greenshaw[20], R.K. Griffiths[21], G. Grindhammer[27], A. Gruber[27], C. Gruber[17], T. Hadig[1], D. Haidt[11], L. Hajduk[6], T. Haller[14], M. Hampel[1], W.J. Haynes[5], B. Heinemann[13], G. Heinzelmann[13], R.C.W. Henderson[19], H. Henschel[36], I. Herynek[31], M.F. Hess[27], K. Hewitt[3], W. Hildesheim[11], K.H. Hiller[36], C.D. Hilton[23], J. Hladký[31], M. Höppner[8], D. Hoffmann[11], T. Holtom[20], R. Horisberger[34], V.L. Hudgson[3], M. Hütte[8], M. Ibbotson[23], H. Itterbeck[1], A. Jacholkowska[28], C. Jacobsson[22], M. Jaffre[28], J. Janoth[16], D.M. Jansen[14], T. Jansen[11], L. Jönsson[22], D.P. Johnson[4], H. Jung[22], P.I.P. Kalmus[21], M. Kander[11], D. Kant[21], R. Kaschowitz[2], U. Kathage[17], J. Katzy[15], H.H. Kaufmann[36], O. Kaufmann[15], M. Kausch[11], S. Kazarian[11], I.R. Kenyon[3], S. Kermiche[24], C. Keuker[1], C. Kiesling[27], M. Klein[36], C. Kleinwort[11], G. Knies[11], T. Köhler[1], J.H. Köhne[27], H. Kolanoski[36,41], S.D. Kolya[23], V. Korbel[11], P. Kostka[36], S.K. Kotelnikov[26], T. Krämerkämper[8], M.W. Krasny[6,30], H. Krehbiel[11], D. Krücker[27], H. Küster[22], M. Kuhlen[27], T. Kurča[36], J. Kurzhöfer[8], D. Lacour[30], B. Laforge[9], M.P.J. Landon[21], W. Lange[36], U. Langenegger[37], A. Lebedev[26], F. Lehner[11], S. Levonian[29], G. Lindström[12], M. Lindstroem[22], F. Linsel[11], J. Lipinski[13], B. List[11], G. Lobo[28], P. Loch[11,43], J.W. Lomas[23], G.C. Lopez[12], V. Lubimov[25], D. Lüke[8,11], L. Lytkin[14], N. Magnussen[35], E. Malinovski[26], R. Maraček[18], P. Marage[4], J. Marks[24], R. Marshall[23], J. Martens[35], G. Martin[13], R. Martin[20], H.-U. Martyn[1], J. Martyniak[6], T. Mavroidis[21], S.J. Maxfield[20], S.J. McMahon[20], A. Mehta[5], K. Meier[16], F. Metlica[14], A. Meyer[11], A. Meyer[13], H. Meyer[35], J. Meyer[11], P.-O. Meyer[2], A. Migliori[29], S. Mikocki[6], D. Milstead[20], J. Moeck[27], F. Moreau[29], J.V. Morris[5], E. Mroczko[6], D. Müller[38], G. Müller[11], K. Müller[11], P. Murín[18], V. Nagovizin[25], R. Nahnhauer[36], B. Naroska[13], Th. Naumann[36], I. Négri[24], P.R. Newman[3], D. Newton[19], H.K. Nguyen[30], T.C. Nicholls[3], F. Niebergall[13], C. Niebuhr[11], Ch. Niedzballa[1], H. Niggli[37], G. Nowak[6], G.W. Noyes[5], T. Nunnemann[14], M. Nyberg-Werther[22], M. Oakden[20], H. Oberlack[27], J.E. Olsson[11], D. Ozerov[25], P. Palmen[2], E. Panaro[11], A. Panitch[4], C. Pascaud[28], G.D. Patel[20], H. Pawletta[2], E. Peppel[36], E. Perez[9], J.P. Phillips[20], A. Pieuchot[24], D. Pitzl[37], G. Pope[7], B. Povh[14], S. Prell[11], K. Rabbertz[1], G. Rädel[11], P. Reimer[31], S. Reinshagen[11], H. Rick[8], F. Riepenhausen[2], S. Riess[13], E. Rizvi[21], S.M. Robertson[3], P. Robmann[38], H.E. Roloff[36,†], R. Roosen[4], K. Rosenbauer[1], A. Rostovtsev[25], F. Rouse[7], C. Royon[9], K. Rüter[27], S. Rusakov[26], K. Rybicki[6], D.P.C. Sankey[5], P. Schacht[27], S. Schiek[13], S. Schleif[16], P. Schleper[15], W. von Schlippe[21],

D. Schmidt[35], G. Schmidt[13], A. Schöning[11], V. Schröder[11], E. Schuhmann[27], B. Schwab[15], F. Sefkow[38], R. Sell[11], A. Semenov[25], V. Shekelyan[11], I. Sheviakov[26], L.N. Shtarkov[26], G. Siegmon[17], U. Siewert[17], Y. Sirois[29], I.O. Skillicorn[10], P. Smirnov[26], V. Solochenko[25], Y. Soloviev[26], A. Specka[29], J. Spiekermann[8], S. Spielman[29], H. Spitzer[13], F. Squinabol[28], P. Steffen[11], R. Steinberg[2], H. Steiner[11,40], J. Steinhart[13], B. Stella[33], A. Stellberger[16], J. Stier[11], J. Stiewe[16], U. Stößlein[36], K. Stolze[36], U. Straumann[15], W. Struczinski[2], J.P. Sutton[3], S. Tapprogge[16], M. Taševský[32], V. Tchernyshov[25], S. Tchetchelnitski[25], J. Theissen[2], C. Thiebaux[29], G. Thompson[21], R. Todenhagen[14], P. Truöl[38], G. Tsipolitis[37], J. Turnau[6], J. Tutas[15], E. Tzamariudaki[11], P. Uelkes[2], A. Usik[26], S. Valkár[32], A. Valkárová[32], C. Vallée[24], D. Vandenplas[29], P. Van Esch[4], P. Van Mechelen[4], Y. Vazdik[26], P. Verrecchia[9], G. Villet[9], K. Wacker[8], A. Wagener[2], M. Wagener[34], B. Waugh[23], G. Weber[13], M. Weber[16], D. Wegener[8], A. Wegner[27], T. Wengler[15], M. Werner[15], L.R. West[3], T. Wilksen[11], S. Willard[7], M. Winde[36], G.-G. Winter[11], C. Wittek[13], M. Wobisch[2], E. Wünsch[11], J. Žáček[32], D. Zarbock[12], Z. Zhang[28], A. Zhokin[25], P. Zini[30], F. Zomer[28], J. Zsembery[9], K. Zuber[16], and M. zurNedden[38]

[1] I. Physikalisches Institut der RWTH, Aachen, Germany[a]

[2] III. Physikalisches Institut der RWTH, Aachen, Germany[a]

[3] School of Physics and Space Research, University of Birmingham, Birmingham, UK[b]

[4] Inter-University Institute for High Energies ULB-VUB, Brussels; Universitaire Instelling Antwerpen, Wilrijk; Belgium[c]

[5] Rutherford Appleton Laboratory, Chilton, Didcot, UK[b]

[6] Institute for Nuclear Physics, Cracow, Poland[d]

[7] Physics Department and IIRPA, University of California, Davis, California, USA[e]

[8] Institut für Physik, Universität Dortmund, Dortmund, Germany[a]

[9] CEA, DSM/DAPNIA, CE-Saclay, Gif-sur-Yvette, France

[10] Department of Physics and Astronomy, University of Glasgow, Glasgow, UK[b]

[11] DESY, Hamburg, Germany[a]

[12] I. Institut für Experimentalphysik, Universität Hamburg, Hamburg, Germany[a]

[13] II. Institut für Experimentalphysik, Universität Hamburg, Hamburg, Germany[a]

[14] Max-Planck-Institut für Kernphysik, Heidelberg, Germany[a]

[15] Physikalisches Institut, Universität Heidelberg, Heidelberg, Germany[a]

[16] Institut für Hochenergiephysik, Universität Heidelberg, Heidelberg, Germany[a]

[17] Institut für Reine und Angewandte Kernphysik, Universität Kiel, Kiel, Germany[a]

[18] Institute of Experimental Physics, Slovak Academy of Sciences, Košice, Slovak Republic[f,j]

[19] School of Physics and Chemistry, University of Lancaster, Lancaster, UK[b]

[20] Department of Physics, University of Liverpool, Liverpool, UK[b]

[21] Queen Mary and Westfield College, London, UK[b]

[22] Physics Department, University of Lund, Lund, Sweden[g]

[23] Physics Department, University of Manchester, Manchester, UK[b]

[24] CPPM, Université d'Aix-Marseille II, IN2P3-CNRS, Marseille, France

[25] Institute for Theoretical and Experimental Physics, Moscow, Russia

[26] Lebedev Physical Institute, Moscow, Russia[f]

[27] Max-Planck-Institut für Physik, München, Germany[a]

[28] LAL, Université de Paris-Sud, IN2P3-CNRS, Orsay, France

[29] LPNHE, Ecole Polytechnique, IN2P3-CNRS, Palaiseau, France

[30] LPNHE, Universités Paris VI and VII, IN2P3-CNRS, Paris, France

[31] Institute of Physics, Czech Academy of Sciences, Praha, Czech Republic[f,h]

[32] Nuclear Center, Charles University, Praha, Czech Republic[f,h]

[33] INFN Roma 1 and Dipartimento di Fisica, Università Roma 3, Roma, Italy

[34] Paul Scherrer Institut, Villigen, Switzerland

[35] Fachbereich Physik, Bergische Universität Gesamthochschule Wuppertal, Wuppertal, Germany[a]
[36] DESY, Institut für Hochenergiephysik, Zeuthen, Germany[a]
[37] Institut für Teilchenphysik, ETH, Zürich, Switzerland[i]
[38] Physik-Institut der Universität Zürich, Zürich, Switzerland[i]
[39] Visitor from Yerevan Phys. Inst., Armenia
[40] On leave from LBL, Berkeley, USA
[41] Institut für Physik, Humboldt-Universität, Berlin, Germany[a]
[42] Rechenzentrum, Bergische Universität Gesamthochschule Wuppertal, Wuppertal, Germany[a]
[43] Physics Department, University of Arizona, Tuscon, USA

† Deceased

[a] Supported by the Bundesministerium für Bildung, Wissenschaft, Forschung und Technologie, FRG, under contract numbers 6AC17P, 6AC47P, 6DO57I, 6HH17P, 6HH27I, 6HD17I, 6HD27I, 6KI17P, 6MP17I, and 6WT87P
[b] Supported by the UK Particle Physics and Astronomy Research Council, and formerly by the UK Science and Engineering Research Council
[c] Supported by FNRS-NFWO, IISN-IIKW
[d] Supported by the Polish State Committee for Scientific Research, grant nos. 115/E-743/SPUB/P03/109/95 and 2 P03B 244 08p01, and Stiftung für Deutsch-Polnische Zusammenarbeit, project no. 506/92
[e] Supported in part by USDOE grant DE F603 91ER40674
[f] Supported by the Deutsche Forschungsgemeinschaft
[g] Supported by the Swedish Natural Science Research Council
[h] Supported by GA ČR grant no. 202/93/2423, GA AV ČR grant no. 19095 and GA UK grant no. 342
[i] Supported by the Swiss National Science Foundation
[j] Supported by VEGA SR grant no. 2/1325/96

1 Introduction

At high energies measurements of the energy dependence of real photon-proton cross sections are consistently described by the power law $\sigma_{\gamma p}^{tot} \propto (W^2)^{\lambda}$, where W is the γp centre of mass energy. The power is $\lambda \approx 0.08$ [1, 2] and is found to be universal for all photon or hadron interactions with protons [3]. The virtual photon-proton cross section however, which is at large W related to the structure function F_2 via $\sigma_{\gamma^* p}^{tot} \approx 4\pi^2\alpha/Q^2 \cdot F_2(W^2, Q^2)$, is found to rise fast with increasing W^2 for Q^2 values larger than a few GeV^2 [4, 5]. Here Q^2 is the virtuality of the photon and α the fine structure constant. At large W the relation $W^2 = Q^2/x$ holds, with x the deep inelastic scattering (DIS) variable Bjorken-x. In the HERA regime fits of the form $\sigma_{\gamma^* p}^{tot} \propto (W^2)^{\lambda}$ lead to values of λ which rise from 0.2 to 0.4 in the Q^2 range from 1.5 to 10^3 GeV^2 [4].

In Regge theory the energy dependence of the total cross sections is specified by the intercept, which is simply $1 + \lambda$, of the pomeron, the leading exchanged trajectory. It is argued (see e.g. [6, 7]) that the change of slope parameter λ with increasing Q^2 is associated with a transition from a non-perturbative 'soft' to a perturbative 'hard' regime. Indeed, in the domain where Q^2 is larger than a few GeV^2 and perturbative QCD can be safely applied, it predicts an increase of λ with Q^2. In the domain of 'soft' interaction phenomenology the change of the slope parameter can be interpreted in Reggeon Field Theory as a reduction of screening corrections with increasing Q^2 [8]. Presently Reggeon Field Theory and perturbative QCD are two complementary approaches which successfully describe physics processes in different regimes, but the transition region between these soft and hard regimes is poorly understood. HERA provides an ideal testing ground to study the transition from soft to hard physics by comparing real and virtual photon-proton collisions in the same experiment. Comparisons of the energy dependence of the cross section or of the final states properties (e.g. multiplicities, energy flows, inclusive particle distributions) allow more insight to be gained into the dynamics of strong interactions and can be helpful in the development of a common underlying picture in terms of an effective field theory (see e.g. [9]).

In a previous publication energy flow in the photon fragmentation region was studied [10]. In this paper we investigate the energy behaviour of the cross section for photoproduction events containing charged particles with high transverse momentum, p_t, and compare it with the energy behaviour of the total inclusive $\gamma^* p$ cross section. The presence of a high p_t charged particle allows a scale to be identified which can be varied in a similar way as the scale in virtual photon interactions, and the effect on the energy dependence of the cross section can be studied. A continuous coverage of both the soft and hard scattering domains becomes possible. To emulate the kinematical configuration of a $\gamma^* p$ collision as closely as possible the high p_t charged track is required to be in the photon fragmentation region, which corresponds at the same time to the largest acceptance region of the H1 tracking detectors. The idea of the analysis is illustrated in Fig.1, where both the virtual and real photon processes are shown, as well as the region of track acceptance.

2 Detector and Data Sample

The data for this analysis were collected by the H1 experiment in 1994, when HERA operated with 27.5 GeV positrons and 820 GeV protons, thus producing e^+p interactions

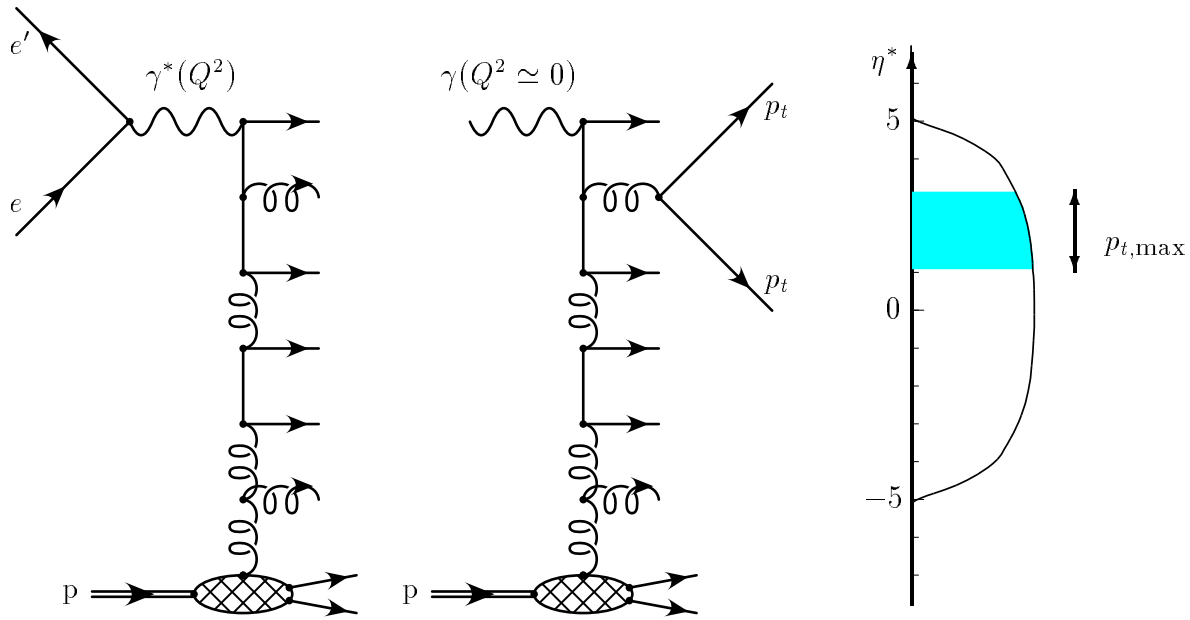

Figure 1: Illustration of diagrams for a DIS event and photoproduction event with high p_t particles in the final state. The sketch on the right side illustrates an inclusive charged particle pseudorapidity distribution in the γp centre of mass system, with the range used to search for high p_t tracks. For real photon interactions all contributing processes (direct, resolved, vector meson production, ...) are considered.

at a centre of mass energy of $\sqrt{s} = 300$ GeV. A detailed description of the H1 apparatus can be found elsewhere [11]. The detector covers almost 4π of the solid angle and consists, moving outwards from the interaction point, of tracking detectors, calorimeters and muon detectors. Along the beam line several other dedicated detectors, such as the luminosity system, have been installed. This analysis makes use of the luminosity system and the central tracking detector.

The scattered positron was detected in the electron tagger of the H1 luminosity system. The system consists of two TlCl/TlBr crystal calorimeters, installed in the HERA tunnel, each having a resolution of $\sigma(E)/E = 0.1/\sqrt{E}$ with E in GeV. The electron tagger is located at $z = -33$ m and the photon tagger at $z = -103$ m from the interaction point in the direction of outgoing positron beam. The energy scale of both calorimeters is known to better than 1.5% [12]. The acceptance of the electron tagger is confined to the kinematical range of $0.2 < y < 0.8$ and $Q^2 < 0.01$ GeV^2. Here y is the fractional energy of the photon and can be well approximated by $y = 1 - E'_e/E_e$, with E_e, E'_e the energies of the initial and scattered positrons respectively. The photon tagger accepts photons with $\pi - \theta < 0.45$ mrad. Here θ is defined with respect to the incident proton direction.

The charge and momentum of charged particles were measured by two coaxial cylindrical drift chambers (central jet chamber, CJC), which cover the polar angular range $15° < \theta < 165°$. A superconducting solenoid provides a uniform magnetic field of 1.15 T parallel to the beam axis in the tracking region. The p_t and θ resolutions of the CJC are $\sigma_{p_t}/p_t \approx 0.009 \cdot p_t$ [GeV] $\oplus$ 0.015 and $\sigma_\theta = 20$ mrad respectively.

Photoproduction events were triggered by a coincidence of an energy deposit larger than ~ 5 GeV in the electron tagger and one or more track candidates with $p_t > 0.4$

GeV from the CJC trigger [13]. In order to reduce the non-ep background contamination and to ensure good reconstruction of the event kinematics, the following selection criteria have been applied for this analysis:

- The event vertex reconstructed from the tracks of charged particles was required to lie within ± 30 cm of the mean z-position of the interaction point, corresponding to a 3σ cut on the interaction region defined by the longitudinal size of the proton bunch.
- In order to suppress random coincidences between the high rate of Bethe-Heitler events $ep \to ep\gamma$ and p-gas background in the main H1 detector, events were rejected if a photon with an energy $E_\gamma > 2$ GeV was detected in the photon tagger. This cut also reduces QED radiative corrections to the ep Born cross section [1].
- The y range was limited to $0.25 < y < 0.70$ to avoid regions of low electron tagger acceptance [1]. This corresponds to photon-proton collision energies of $150 < W = \sqrt{ys} < 250$ GeV.
- To ensure a good measurement of the scattered positron energy, a fiducial cut was applied to reject events with a positron detected close to the acceptance boundaries of the electron tagger.

In total $1.8 \cdot 10^6$ events satisfy the above selection criteria, from a data sample which corresponds to an integrated luminosity of $\mathcal{L} = 2.6$ pb^{-1}. The residual background contamination was estimated to be $(2.4 \pm 0.5)\%$.

The data were divided into several sub-samples according to the charged particle with the maximum transverse momentum, $p_{t,\max}$, found in the pseudorapidity range $1.1 < \eta^* < 3.1$. Here pseudorapidity is defined in the photon-proton centre of mass system as $\eta^* = -\ln\tan(\theta^*/2)$ with the polar angle θ^* measured with respect to the photon direction. The pseudorapidity interval chosen corresponds to a region in the detector which guarantees a good track measurement in the CJC and a uniform track acceptance over the whole W range studied. Only those tracks were considered which have $p_t > 0.15$ GeV, are fitted to the primary event vertex and further satisfy a number of quality criteria detailed in Ref. [14]. The systematic error due to the track selection was estimated by varying these quality criteria in a wide range and repeating the complete analysis. In total eleven bins in $p_{t,\max}$ have been defined, covering the $p_{t,\max}$ range from 0.5 to 7 GeV. The bin sizes were determined to have adequate statistics and such that the size is always larger than four times the p_t resolution in the bin to minimize migration effects. The values of the $p_{t,\max}$ boundaries for the bins are indicated in Fig. 2.

The track reconstruction efficiency, the contamination from secondary vertices and decays close to the primary vertex, and residual bin-to-bin migrations have been determined from Monte Carlo studies. Events were generated with the PYTHIA model [15] and passed through the full H1 detector simulation. All simulated events were subjected to the same reconstruction and selection procedure as the real data. The migration effects were found to be small, between 10% and 20%, and the ratio of the number of reconstructed to the number of generated events to be close to one ($\pm 4\%$) in all $p_{t,\max}$ bins.

3 Results and Discussion

In ep collisions, for any sub-class i of photoproduction events the energy dependence $\sigma^i_{\gamma p}(W)$ can be extracted from the corresponding differential ep cross section using the Weizsäcker-Williams formula [16] for the photon flux $F(y, Q^2)$. After integrating over Q^2, the corresponding relation reads:

$$\frac{dN^i_{ep}}{dy} = (1 + \delta_{RC})\ \mathcal{L}\ F(y)\ A(y)\ \epsilon^i(y)\ \sigma^i_{\gamma p}(W), \tag{1}$$

where N^i_{ep} denotes the observed number of events belonging to class i, $\mathcal{L}$ is the integrated luminosity, $A(y)$ is the acceptance of the electron tagger and $\epsilon^i(y)$ is the efficiency of the trigger and selection criteria. The factor $(1 + \delta_{RC})$ is a correction for the cross section for QED radiation to obtain the ep Born cross section.

The main systematic uncertainty, which so far prevents an accurate measurement of the energy dependence of the total photoproduction cross section at HERA, results from the large variation of the tagging acceptance $A(y)$ (between 0.15 and 0.8 in the W range of interest), and which, in addition, strongly depends on the beam optics [1, 12]. However, the *relative* energy dependence for different photoproduction event classes can be determined with much better precision. Hence we consider the ratio

$$R^i(y) = \frac{\sigma^i_{\gamma p}(W)}{\sigma^{tot}_{\gamma p}(W)} = \frac{dN^i_{ep}/dy}{dN_{ep}/dy} \cdot \frac{\epsilon(y)}{\epsilon^i(y)} \equiv \frac{\tilde{R}^i(y)}{r^i_\epsilon(y)}, \tag{2}$$

where ϵ and ϵ^i denote the efficiencies for all events and for the events in class i respectively, and $\tilde{R}$ is the uncorrected ratio. All efficiencies in (2) cancel except for the trigger efficiency. Hence r^i_ϵ is the ratio of the trigger efficiency for the sample i to that of the full sample.

Applying this method the W dependence of the uncorrected ratio $\tilde{R}$ for each bin i of $p_{t,\max}$ is shown in Fig. 2 together with a power-law fit of the form $\tilde{R} \propto W^{2\cdot\tilde{\lambda}(p_{t,\max})}$.

In order to obtain the energy dependence of the partial cross sections, defined in a $p_{t,\max}$ bin with width 2Δ,

$$\sigma^i_{\gamma p}(W) \equiv \sigma_{\gamma p}(W, p^2_{t,\max}) = \int_{p_{t,\max}-\Delta}^{p_{t,\max}+\Delta} d\sigma_{\gamma p}(W)/dp_{t,\max} \cdot dp_{t,\max}$$

in (2) the parameters $\tilde{\lambda}(p_{t,\max})$ have been corrected for trigger efficiency $r^i_\epsilon(y)$ and account has been taken of the energy dependence of the total cross section in the denominator of (2):

$$\lambda_{\gamma p}(p_{t,\max}) = \tilde{\lambda}(p_{t,\max}) - \lambda_\epsilon(p_{t,\max}) + \lambda_{I\!P} \tag{3}$$

where $\lambda_\epsilon(p_{t,\max})$ is the trigger efficiency correction and $\lambda_{I\!P} = 0.08 \pm 0.03$. The rather conservative error assigned to $\lambda_{I\!P}$ accounts for the invisible part of the total γp cross section with the data selection of this analysis (mainly elastic and low-mass diffractive dissociation processes) [1]. The correction due to the trigger efficiency was obtained directly from the data, using a sub-sample taken with a trigger based solely on calorimetric quantities. Correlated systematic errors of the $r^i_\epsilon(y)$ largely cancel in the measurement of the slope parameter $\lambda_{\gamma p}$. The contributions of the systematic errors to the total error $\delta\lambda_{\gamma p}$, excluding the overall uncertainty in $\lambda_{I\!P}$, are summarized in Table 1. The rightmost

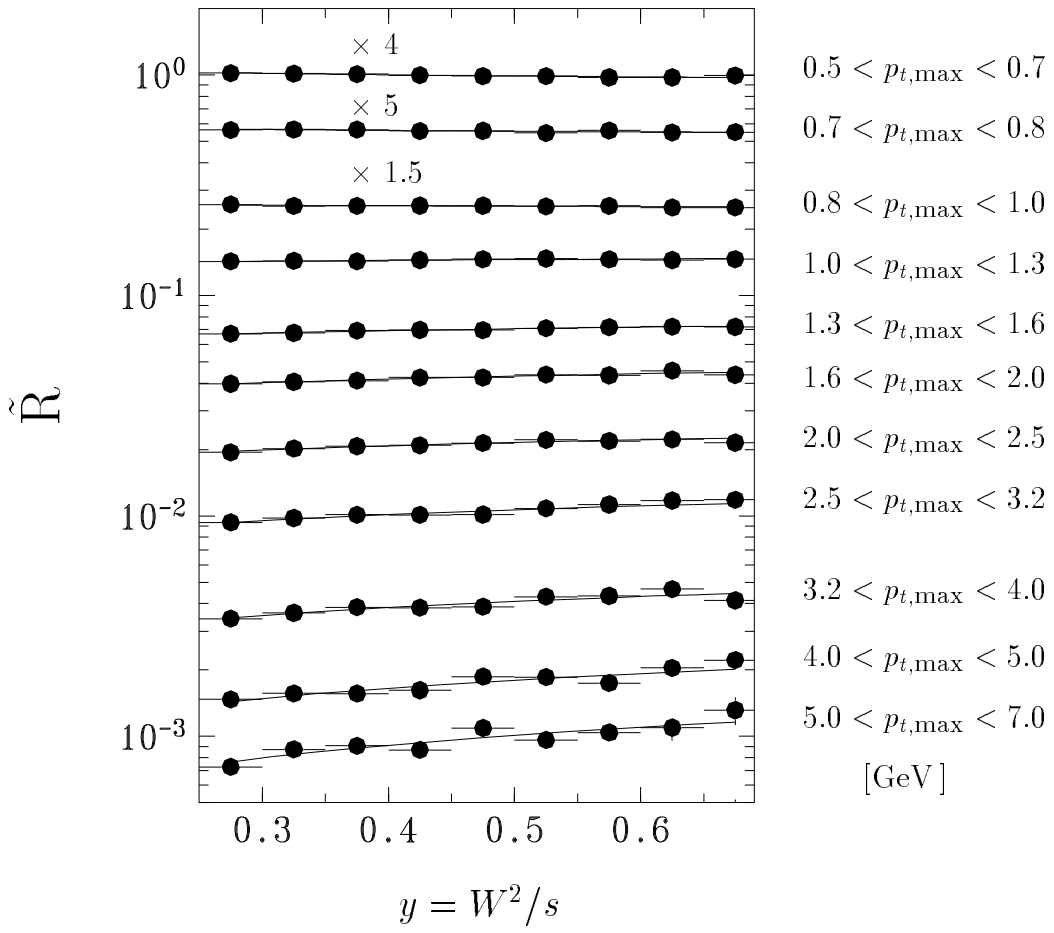

Figure 2: The energy dependence of the ratio $\tilde{R}$ in different bins of the $p_{t,\max}$ of the charged particles produced in the pseudorapidity window $1.1 < \eta^* < 3.1$. The curves represent a fit of the form $\tilde{R} \propto W^{2 \cdot \tilde{\lambda}(p_{t,\max})}$ motivated by the Regge formalism. For visibility the data of the three lowest $p_{t,\max}$ bins are multiplied with the factors indicated in the figure.

column gives the systematic error resulting from the precision of the W^2 reconstruction and the stability of the power-law fit to variations of the W^2 range used.

The final corrected values of $\lambda_{\gamma p}(p_{t,\max})$ are plotted in Fig.3a against the scale which is chosen to be $(2p_{t,\max})^2$. The statistical errors dominate the precision of the $\lambda_{\gamma p}(p_{t,\max})$ measurement in the high-p_t range ($p_{t,\max} > 3$ GeV).

A fit to the data of the form $\lambda_{\gamma p}(p_{t,\max}) = C \cdot \ln(4p_{t,\max}^2) + \lambda_0$ with full errors except for $\delta\lambda_{I\!P}$ (full straight line on Fig.3a) gives a $\chi^2/ndf = 0.3$ with $C = 0.112 \pm 0.007$ and $\lambda_0 = 0.031 \pm 0.014$. Note that when the scale $4p_{t,\max}^2$ is multiplied with a constant, this does not change the slope C of the scale dependence, but only influences the value of λ_0. Thus the change of $\lambda_{\gamma p}(p_{t,\max})$ with the scale has physical significance.

Fig.3a shows also predictions of a longitudinal phase space model (LPS) and of the PYTHIA model [15]. The PYTHIA model is based on perturbative QCD for the hard scattering processes, but also includes a Regge inspired soft interaction component. For

Table 1: Values and the systematic error summary for the measurement of the slope parameter $\lambda_{\gamma p}(p_{t,\max})$. The overall systematic error $\delta\lambda_{I\!P} = 0.03$ is not included in this table, but is included in Fig.3a.

Bin	$< p^2_{t,\max} >$ [GeV^2]	$\lambda_{\gamma p}(p_{t,\max}) \pm \delta\lambda_{\gamma p}(stat)$	Systematic errors		
			track sel.	trigger	W^2 fit
1	0.36	0.080 ± 0.006	0.001	0.02	0.006
2	0.56	0.121 ± 0.009	0.001	0.01	0.008
3	0.80	0.157 ± 0.007	0.001	0.01	0.007
4	1.29	0.211 ± 0.008	0.002	0.01	0.004
5	2.06	0.267 ± 0.012	0.001	0.01	0.004
6	3.14	0.334 ± 0.015	0.001	0.01	0.007
7	4.90	0.344 ± 0.022	0.001	0.01	0.003
8	7.77	0.407 ± 0.031	0.001	0.01	0.006
9	12.46	0.484 ± 0.051	0.015	0.02	0.008
10	19.56	0.565 ± 0.079	0.036	0.03	0.004
11	33.43	0.603 ± 0.105	0.071	0.07	0.062

the LPS model particles were generated with a uniform distribution in rapidity, taking into account energy-momentum constraints, and with a transverse momentum distribution $d\sigma/dp_t^2 \propto (p_t^2 + p_0^2)^{-n}$ with $p_0 = 0.5$ GeV and $n = 2.9$, tuned to describe the charged particle multiplicity and p_t spectra of the data in the photon fragmentation region. As expected, phase space effects start to become important only at very large $p_{t,\max}$ values and cannot explain the trend observed in the data. PYTHIA, on the other hand, describes the data well. In studying the different ingredients in this model it turns out that the main part of the rise can be explained by the integration of the leading order matrix elements over the available phase space. This is in agreement with expectations reported in [17]. Since this integration is regulated by the quantity $p_t^2/\hat{s}$, with $\hat{s}$ the invariant mass squared of the hard scattering subsystem, the rise for a given $p_{t,\max}$ value will depend on the W range studied. Parton showers, simulating next to leading order effects, as well as multiple parton-parton scattering, account for at most 20% of the measured $\lambda_{\gamma p}(p_{t,\max})$. The effects of using different proton and photon structure functions are small. Hence the change of $\lambda_{\gamma p}(p_{t,\max})$ is not associated with the growth of the gluon density in the proton at small-x, contrary to naive expectation.

In Fig.3b the measurement of λ in $\sigma^{tot}_{\gamma^* p} \propto (W^2)^{\lambda_{DIS}(Q^2)}$ is shown for the virtual-photon proton cross section as function of the virtuality Q^2 [4]. For DIS the Q^2 dependence of $\lambda_{DIS}(Q^2)$ is qualitatively described by perturbative QCD, as shown in Fig. 3b by the calculations for two quite different proton structure function parametrisations [18, 19]. Both are based on the DGLAP evolution equations [20] but assume a different x-behaviour at the starting scale, Q_0^2, of the evolution. At $Q^2 \sim 4$ GeV^2 the MRS-D0′ parton densities are constant in x ($\lambda \sim 0$), while for GRV they are singular at $x = 0$ ($\lambda > 0$). This difference is reflected in the predictions for the GRV and MRS-D0′ parametrisations in Fig. 3b. However, both predict a significant rise of $\lambda_{DIS}(Q^2)$ with Q^2, due to the singular behaviour of the box diagram $g \to q\overline{q}$ of the DGLAP evolution kernel [21]. In detail neither of the two calculations agrees very well with the data which are in between the predictions. Note that the MRS-D0′ distributions were found to be in disagreement with the structure function data itself [4, 5].

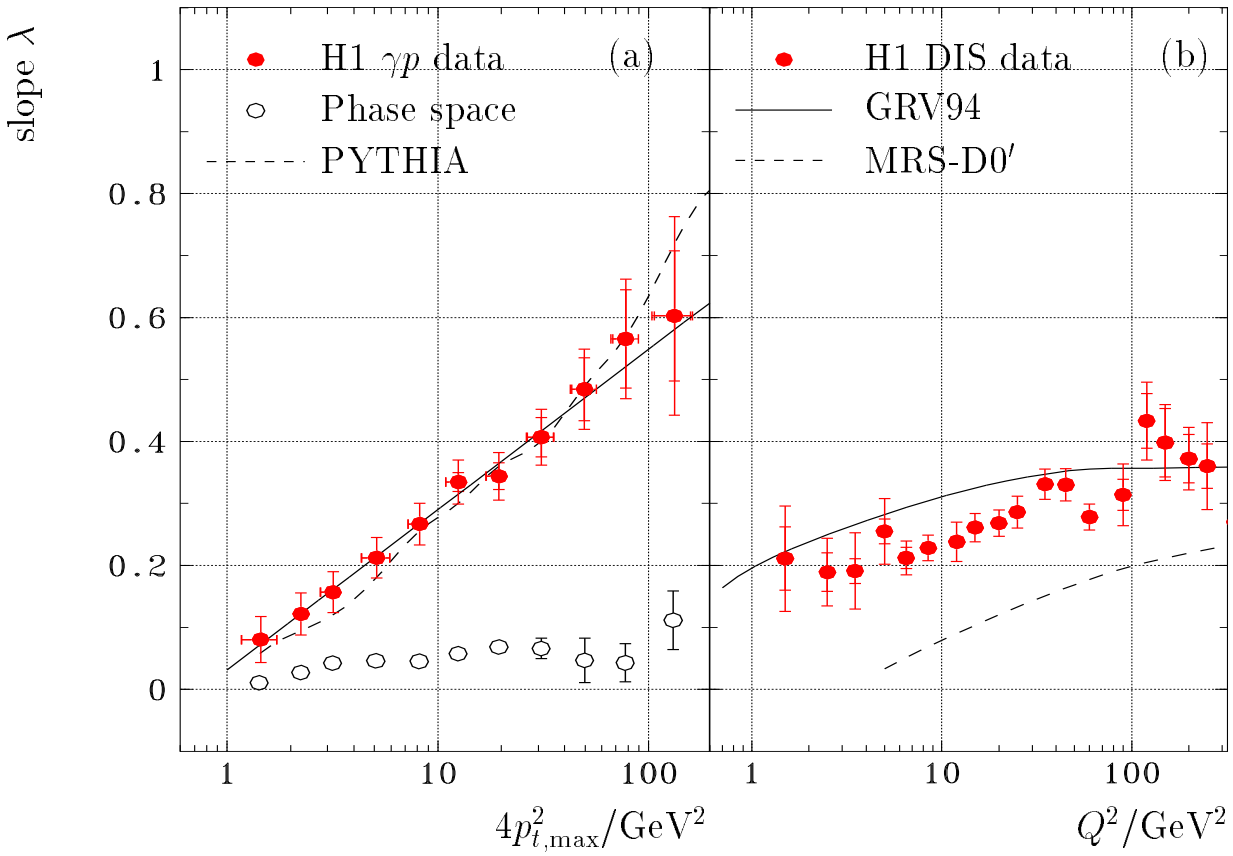

Figure 3: a) The scale dependence of the slope $\lambda_{\gamma p}(p_{t,\max})$ in photoproduction (full points). The full line represents the result of a linear fit $\lambda_{\gamma p}(p_{t,\max}) = C \cdot \ln(4p_{t,\max}^2) + \lambda_0$ to the data. The dashed line is the prediction from PYTHIA and the open points are the prediction from a longitudinal phase space model. b) The scale dependence of the slope $\lambda_{DIS}(Q^2)$ in deep inelastic data compared to different parametrisations of the proton structure function F_2: full line GRV, dashed line MRS-D0′. For both figures inner error bars show the statistical errors; full error bars correspond to statistical and systematic errors added in quadrature.

A qualitative similarity is seen between the W dependence of the cross sections for high-p_t particle photoproduction and for deep inelastic scattering: they both show a significant rise of $\lambda_{\gamma p}(p_{t,\max})$ and $\lambda_{DIS}(Q^2)$ with increasing scale. The use of different scales in the study of this effect in the two processes prevents however a direct quantitative comparison. The range of the scale is varied from 1 GeV^2 to 100 GeV^2 and within that range the rise of the slope parameter is stronger for $\sigma_{\gamma p}(W, p_{t,\max}^2)$. In view of the discussion above the rise in both processes can be understood as follows:

- Perturbative QCD : as argued above, the rise of the cross section for photoproduction events with a high p_t particle can be explained in terms of parton-parton scattering. On the other hand, the rise of the slope parameter due to QCD evolution in DIS can be traced to the singular behaviour of the box diagram describing the elastic $\gamma^* p$ scattering amplitude. This diagram gives the contribution to the $\gamma^* p$ cross section of photon-parton scattering with gluon or quark radiation and can be expected to have similar properties as the diagrams for parton-parton scattering in high p_t

photoproduction. It can be shown [22] that the photon-gluon fusion diagram leads to a rise of F_2 which is compatible with the HERA data [23]. Hence, in view of Fig. 1, the cross section evolution with the scale (p_t^2 in photoproduction and Q^2 in DIS) can then be readily explained by leading order partonic scattering contributions.

- Regge approach: in Reggeon Field Theory, high energy particle interactions are described by pomeron exchange and λ is related to the pomeron intercept. At high energies the unitarity corrections to the one-pomeron exchange, which effectively reduce the cross section value, become important. It has been shown [24] that these reduce the value of λ. In both cases studied here the cross sections are far below the unitarity bound [25] and in a region where unitarity corrections become gradually smaller [8]. Hence the cross section can rise faster with W for either increasing p_t^2 or Q^2. The data shows that this is indeed the case and the development of the rise is similar, albeit not identical, for both cases.

In short, an interesting similarity is observed in the evolution of the energy dependence of $\sigma_{\gamma p}(W, p^2_{t,\max})$ and $\sigma^{tot}_{\gamma^* p}(W, Q^2)$, in qualitative agreement with leading order perturbative QCD and Regge Field Theory expectations. When decreasing the scale from large values towards 1 GeV^2, which corresponds to a $p_{t,\max}$ of 0.5 GeV, no clear change is observed in the scale dependence of $\lambda_{\gamma p}(p_{t,\max})$. Hence the evolution towards the soft region appears to be rather smooth.

4 Conclusion

A significant change is measured in the energy dependence of the partial cross section $\sigma_{\gamma p}(W, p^2_{t,\max})$ with increasing transverse momentum of the charged particles in the photon fragmentation region. This result cannot be described by a simple longitudinal phase space model. It is, however, well reproduced by leading order QCD and can be qualitatively understood in the framework of Reggeon Field Theory. A similarity is observed in the behaviour of the energy dependence of the $\sigma_{\gamma p}(W, p^2_{t,\max})$ and $\sigma^{tot}_{\gamma^* p}(W, Q^2)$. This supports a common underlying picture for real and virtual photoproduction as well as a smooth and continuous transition from hard to soft processes.

Acknowledgments

We are grateful to the HERA machine group whose outstanding efforts made this experiment possible. We appreciate the immense effort of the engineers and technicians who constructed and maintain the H1 detector. We thank the funding agencies for financial support. We acknowledge the support of the DESY technical staff. We wish to thank the DESY directorate for the support and hospitality extended to the non-DESY members of the collaboration. We thank A. Kaidalov and E. Levin for stimulating discussions.

References

[1] H1 Collab., S. Aid et al., Z.Phys. C69 (1995) 27.

[2] ZEUS Collab., M. Derrick et al., Z.Phys. C63 (1994) 391.

[3] A. Donnachie and P.V. Landshoff, Phys.Lett. B296 (1992) 227;
H. Cheng, J.K. Walker, and T.T. Wu, Phys.Lett. B44 (1973) 97.

[4] H1 Collab., I. Abt et al., Nucl.Phys. B407 (1993) 515;
H1 Collab., T. Ahmed et al., Nucl.Phys. B439 (1995) 471;
H1 Collab., S. Aid et al., Nucl. Phys. B470 (1996) 3.

[5] ZEUS Collab., M. Derrick et al., Phys.Lett. B316 (1993) 412;
ZEUS Collab., M. Derrick et al., Z.Phys. C65 (1995) 379;
ZEUS Collab., M. Derrick et al., Z.Phys. C69 (1996) 607.

[6] J. Bartels, Proceedings of the Workshop on Deep-Inelastic Scattering and QCD, Eds. Y. Sirois and J.F. Laporte, Paris (1995) 105.

[7] A. Levy, to appear in Proceedings of the Workshop on Deep-Inelastic Scattering and Related Phenomena, Eds. G. D'Agostini and A. Nigro, Rome, April 1996.

[8] A. Capella, A. Kaidalov, C. Merino and J. Tran Thanh Van, Phys.Lett. B337 (1994) 358.

[9] L. Lipatov, Proceedings of the Workshop on Deep-Inelastic Scattering and QCD, Eds. Y. Sirois and J.F. Laporte, Paris (1995) 153.

[10] H1 Collab., S. Aid et al., Phys.Lett. B358 (1995) 412.

[11] H1 Collab., I. Abt et al., "The H1 detector at HERA", DESY H1-96-01 (1995), accepted for publication in Nucl.Instr. and Meth.

[12] H1 Collab., T. Ahmed et al., Z.Phys. C66 (1995) 529.

[13] T. Wolff et al., Nucl.Instr. and Meth. A323 (1992) 537.

[14] H1 Collab., S. Aid et al., DESY preprint 096-122.

[15] T. Sjöstrand, CERN-TH-6488 (1992), Comp. Phys. Commun. 82 (1994) 74.

[16] C.F. Weizsäcker, Z.Phys. 88 (1934) 612;
E.J. Williams, Phys.Rev. 45 (1934) 729;
S. Frixione et al., Phys.Lett. B319 (1993) 339.

[17] D. Cline, F. Halzen and J. Luthe, Phys.Rev.Lett. 31 (1973) 491.

[18] M. Glück, E. Reya and A. Vogt, Z.Phys. C67 (1995) 433;
A. Vogt, Proceedings of the Workshop on Deep-Inelastic Scattering and QCD, Eds. Y. Sirois and J.F. Laporte, Paris (1995) 261.

[19] A.D. Martin, R.G. Roberts and W.J. Stirling, Phys.Lett. B306 (1993) 145.

[20] V.N. Gribov and L.N. Lipatov, Sov.J.Nucl.Phys. 15 (1972) 438;
G. Altarelli and G. Parisi, Nucl.Phys. B126 (1977) 298.

[21] John C. Collins (Illinois Tech. and Argonne), Illinois Tech. preprint-86-0298 (1986), Published in UCLA SSC Workshop, Eds. H.-U. Bengtsson, C. Buchanan, T. Gottschalk and A. Soni (1986) 15.

[22] R.D. Field, *Applications of Perturbative QCD* (Addison Wesley, New York, 1989).

[23] W. Buchmüller and D. Haidt, DESY preprint DESY 96-061 (1996).

[24] A.B. Kaidalov, L.A. Ponomarev and K.A. Ter-Martirosyan, Sov.J.Nucl.Phys. 44 (1986) 468.

[25] A.L. Ayala, M.B. Gay Ducati and E.M. Levin, ANL preprint ANL-HEP-PR-96-52 (1996).